Optical Materials 33 (2011) 1829–1832

Contents lists available at ScienceDirect

Optical Materials

journal homepage: www.elsevier.com/locate/optmat

# Synthesis and photoluminescence of ultra-pure germanium nanoparticles

R. Chivas [a,*], S. Yerci [a,1], R. Li [a,2], L. Dal Negro [a,b], T.F. Morse [a,b]

[a] Boston University Photonics Center, Department of Electrical and Computer Engineering, 8 Saint Mary's Street, Boston, MA 02215, USA
[b] Division of Materials Science and Engineering, 15 Saint Mary's Street, Brookline, MA 02446, USA

ARTICLE INFO

*Article history:*
Received 22 February 2011
Received in revised form 10 July 2011
Accepted 5 August 2011

*Keywords:*
Nanocrystals
Light emission
Germanium materials
Aerosol synthesis

ABSTRACT

We have used aerosol deposition to synthesize defect and micro-strain free, ultra-pure germanium nanoparticles. Transmission electron microscopy images show a core–shell configuration with highly crystalline core material. Powder X-ray diffraction measurements verify the presence of highly pure, nano-scale germanium with average crystallite size of 30 nm and micro-strain of 0.058%. X-ray photoelectron spectroscopy demonstrates that $GeO_x$ ($x \leqslant 2$) shells cover the surfaces of the nanoparticles. Under optical excitation, these nanoparticles exhibit two separate emission bands at room temperature: a visible emission at 500 nm with 0.5–1 ns decay times and an intense near-infrared emission at 1575 nm with up to ~20 μs lifetime.



## 1. Introduction

The study of light emission from nanoscale structures based on group IV semiconductors can lead to the demonstration of efficient visible and near-infrared light sources. To this purpose, silicon nanocrystals (Si-ncs) have been primarily investigated in the last ten years, both theoretically [1,2] and experimentally [3,4]. It is now generally accepted that both quantum confinement and surface passivation effects play crucial roles in the photoluminescence (PL) and optical gain properties of silicon nanocrystals [1–7]. Compared to Si, light emission from Ge nanocrystals (Ge-ncs) has not been intensively investigated, and the mechanism of light emission in Ge-ncs is still not fully understood. Recently, it has been predicted from *ab initio* calculations [8] that the optical properties of Ge-ncs should remain typical of an indirect gap semiconductor (i.e. long radiative lifetime) over a wide range of sizes, in spite of the small difference (0.14 eV) between direct and indirect gaps of bulk Ge. To date, Ge-ncs have been fabricated by several methods, ranging from ion-implantation [9], MBE growth [10], co-sputtering [11], sol–gel synthesis [11], chemical reduction of $Si_{0.75}Ge_{0.25}O_2/Si_{0.75}Ge_{0.25}$ [12], electrochemical etching [13], and organic synthesis [14]. However, depending on the specific fabrication conditions, low quantum-yield visible (blue–green) and near-infrared (0.88 eV) PL bands have been observed in Ge-ncs [11,14], with a typical emission lifetime ranging from nanosecond to microsecond time scales, most likely dominated by non-radiative recombination. At present, it is unclear to what extent these results can be unambiguously attributed to nanoscale Ge emission, as opposed to extrinsic factors such as local strain, defect centers, germanium oxide ($GeO_x$, $x \leqslant 2$) layers formation and surface/interface trap states.

In this letter, we demonstrate a novel fabrication approach for the synthesis of ultra-pure, micro-strain free Ge nanoparticles. We investigate their structural characteristics using transmission electron microscopy (TEM), scanning electron microscopy (SEM), powder X-ray diffraction (XRD) and X-ray photoelectron spectroscopy (XPS). Finally, we explore their photoluminescence (PL) and emission relaxation properties.

## 2. Experimental

### 2.1. Synthesis of germanium nanoparticles

Germanium nanoparticles are produced using an aerosol deposition method [15]. In this technique, an ultrasonic transducer (1.6 MHz) nebulizes a liquid precursor solution and the resulting liquid droplets are of the order of 10 μm in diameter. The resulting aerosol is convectively transported by helium gas through the inner volume of a silica glass tube to a reaction zone in a manner similar to the modified chemical vapor deposition (MCVD) method for optical fiber preform doping. As with MCVD, a standard 19 × 25 mm silica tube of high purity simultaneously acts as the furnace and is used as the deposition substrate. Contrary to MCVD, in this case, the liquid precursor has low vapor pressure and consists of tetrapropylgermane, $(C_3H_7)Ge$, mixed with toluene, $C_7H_8$,

* Corresponding author. Present address: Syprosoft Engineering, 1150 Main Street Suite E, Irvine, CA 92614, USA.
*E-mail address:* bchiv05@gmail.com (R. Chivas).
[1] Present address: Department of Mechanical Engineering, Massachusetts Institute of Technology, Cambridge, MA 02139, USA.
[2] Present address: Department of Electrical and Computer Engineering, University of Toronto, 10 King's College Road, Toronto, Ontario, Canada M5S 3G4.

0925-3467/$ - see front matter © 2011 Elsevier B.V. All rights reserved.
doi:10.1016/j.optmat.2011.07.009

in a liquid aerosol. Thus the only atoms participating in the synthesis are Ge, C and H. A localized hot zone created externally with an oxy-hydrogen torch initiates synthesis of pure germanium nanoparticles which are deposited along the inner surface of the silica tube downstream by thermophoresis. The result of the reaction is not a thin film but a layer of solid nanoparticles that are then mechanically removed from the glass substrate. Since they are formed away from the side walls, the properties of the Ge nanoparticles do not depend on the substrate.

### 2.2. Measurement

The material composition was confirmed by detailed powder XRD (PANalytical X'Pert Pro) and XPS analysis (Kratos). Field Emission-SEM (Zeiss Supra 40) and TEM (Joel 2010) measurements confirmed the synthesized material morphology. XRD scans were taken between 20° and 140° with 0.01671°/step in standard $2\Theta$ geometry. Diffraction peak broadening was measured by profile fitting peaks using a Pearson VII function and then deconvoluting the instrument profile from the integral breadth of the peak [16]. Williamson–Hull analysis of the peak allowed contributions from crystallite size broadening and micro-strain broadening to be separated [17]. XPS measurements were performed using Al $K_\alpha$ line (1486.6 eV) as an X-ray source with a power of 150 W. XPS signals of Si, O, C and Ge atoms were recorded with a pass energy of 20 eV. The PL characterization was performed under continuous wave (CW) and pulsed excitations. In the near infrared CW PL experiments, the 488 nm line of an Ar laser (Spectra Physics, 177-G02) modulated with square waves by an acousto-optic modulator was used as the excitation source. The PL was detected using a liquid nitrogen cooled Hamamatsu NIR photo-multiplier tube (PMT) (R5509-73) attached to a spectrometer (Cornerstone 260). Decay times in the near infrared were measured using an oscilloscope coupled to the PMT. The spectral range was limited to below 1700 nm. The visible time-resolved PL measurements were performed using a frequency doubled, tunable Ti:Sa laser with 100 fs pulse duration (Spectra Physics, MaiTai HP). The excitation wavelength was 400 nm and the laser repetition rate was decreased to 5 MHz using an electro-optic modulator (Conoptics 350-160). The emitted light was spectrally resolved by a spectrometer (f/4, Acton) and detected by a ps-resolution Streak camera operating in the photon counting mode (Hamamatsu C4780). All the PL spectra shown in this work have been corrected by the measured response curve of the experimental set-up.

## 3. Results and discussion

Fig. 1 is composed of electron microscopy images detailing the morphology of Ge nanoparticles individually, as well as in powder. In Fig. 1a, the SEM image shows a cluster of agglomerated and unagglomerated Ge nanoparticles whose sizes vary significantly in the 10–100 nm range. The slightly defocused TEM image in Fig. 1b records multiple diffraction planes of the nanoparticles demonstrating their crystalline nature. Crystallite twinning is represented by multiple sets of parallel lines as a result of electron diffraction contributions from randomly oriented lattice planes of germanium crystallites. In the inset of Fig. 1b a TEM image shows that the particles are surrounded by ~5 nm layer of a covering layer, whose composition is analyzed using XPS (Fig. 2a).

Ge 2p and Ge 3d XPS signals, Shirley background correction and Voigt fits associated to non-oxidized Ge ($Ge^0$), sub-oxides of Ge ($Ge^{n+}$, $n = 1$, 2 and 3) and $GeO_2$ ($Ge^{4+}$) states are shown in Fig. 2a. The XPS signal of non-oxidized Ge is relatively larger for Ge 3d than Ge 2p energy level. Reversely, the signals related to $GeO_2$ and Ge sub-oxides are relatively lower for Ge 3d than Ge 2p energy level.

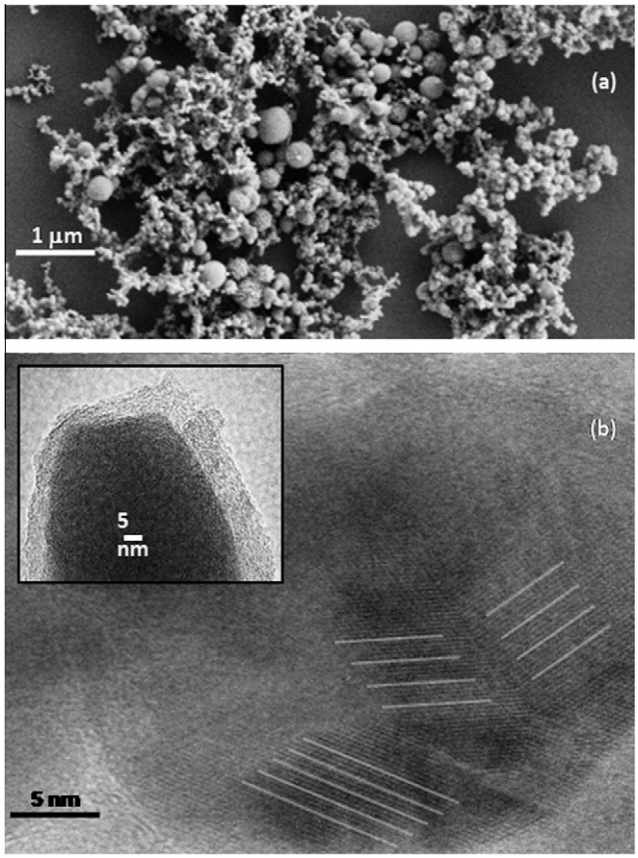


**Fig. 1.** (a) SEM showing a mixture of agglomerated and unagglomerated particles in a range of sizes from 10 to 100 nm. (b) A HRTEM image captures the crystalline nature of the synthesized material. Electron diffraction from randomly oriented germanium lattice planes is represented by sets of dark parallel lines (white lines are drawn as guides to the eye). (inset) TEM image of a single particle highlighting a ~5 nm thick capping layer, identified by XPS analysis as germanium oxide.

It is well-known that the escape depth of a recoiled electron is a function of its kinetic energy (KE) [18]. The escape depths of electrons recoiled from Ge 2p (KE = 268 eV) and Ge 3d (KE = 1458 eV) energy level are approximately 1 nm and 2.5 nm, respectively. In other words, XPS signals of Ge 3d originated from deeper layers than Ge 2p signals. Therefore, one can say that these Ge nano-particles are surrounded by first Ge sub-oxide and then $GeO_2$ shells, in agreement with TEM micro-images.

The powder-XRD data analysis performed on Ge nanoparticles, shown in Fig. 2b, demonstrates an excellent agreement with the calculated Bragg diffraction angles for bulk Ge. Williamson–Hull [17] analysis allowed us to calculate an average crystallite size of 30 nm with a negligible micro-strain of 0.058%, shown in the inset of Fig. 2b. Self-consistent cell refinement for Ge nanoparticles yielded a lattice constant value of 5.6576 Å, comparable to 5.65735 Å as reported by Wyckoff [19]. The standard deviation of the lattice parameter is 0.0001 Å.

The light emission characteristics of ultra-pure Ge nano-powders are displayed in Fig. 3. A broad visible emission band, centered at about 500 nm, can be observed under pulsed excitation at 400 nm in Fig. 3a. The emission relaxation dynamics within this band shows strongly dispersed, nanosecond-fast decay times. All of the decay traces have been fitted using a stretched exponential function. The corresponding PL lifetimes and stretching constants measured at different wavelengths within the PL band are plotted in the inset of Fig. 3a. These results are consistent with a defect-related emission from the Ge-oxide layer surrounding the particle

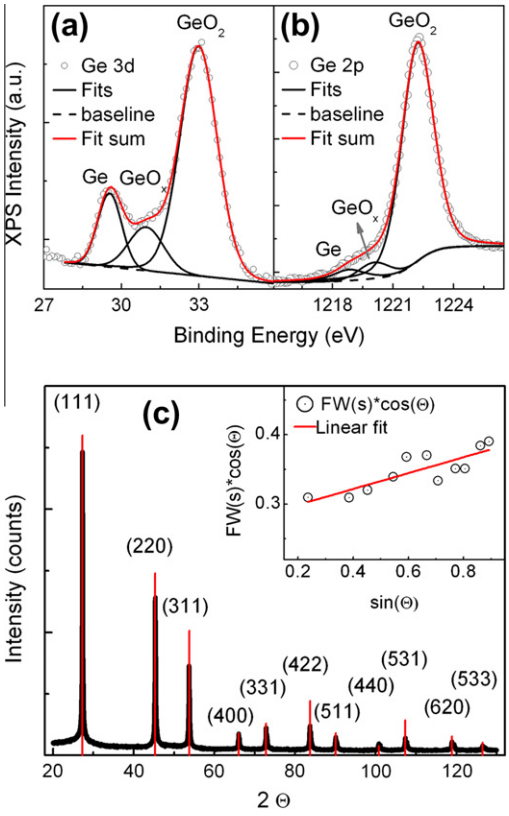


**Fig. 2.** (a) Ge 3d and (b) Ge 2p XPS signals, Shirley background correction and Voigt fits associated to non-oxidized Ge ($Ge^0$), sub-oxides of Ge ($Ge^{n+}$, $n = 1, 2$ and 3) and $GeO_2$ ($Ge^{4+}$) states (c) XRD reflections peaks of Ge nanoparticles superimposed on the calculated reflection angles for bulk germanium. The inset to 2(c) shows the size–strain plot of the particles with average crystallite size, $X(S) = 306$ Å and 0.058% micro-strain.

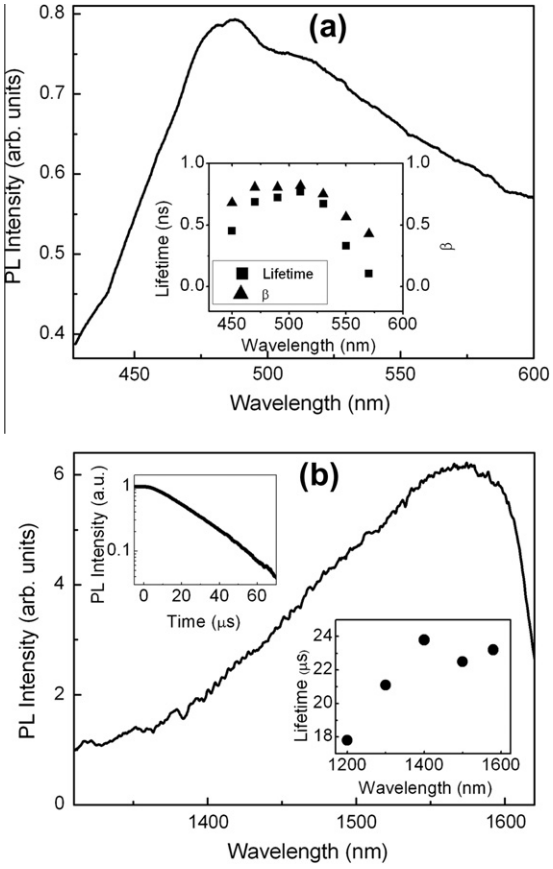


**Fig. 3.** (a) Room temperature photoluminescence under 100 fs pulsed excitation at 400 nm. The average pump power was 5 mW. The emission spectrum has been collected using the analog integration mode of the Hamamatsu streak camera. (inset) Emission decay times (squares) and stretched exponential constants (triangles) detected at different wavelengths within the visible emission range of the sample. (b) Near-infrared emission band measured at room temperature under continuous-wave (CW) excitation at 488 nm. The average pump power was 5 mW. (upper inset) Room temperature emission decay times measured in the near-infrared emission band. In the lower inset, we show five representative emission decay traces corresponding to different wavelengths, as written in the legend.

surfaces, as reported in the literature [20] and consistent with our XPS analysis. The stretched exponential nature of the emission lifetimes measured in the visible can be explained by the structural inhomogeneities and non-stoichiometry (chemical disorder) of the Ge nanoparticle surfaces. In addition to this visible emission band, an intense near-infrared emission is also observed at room temperature under CW pumping, as shown in Fig. 3b. A broad PL spectrum is collected from 1000 nm to approximately 1700 nm. Peak emission is near 1575 nm where the PMT detector sensitivity limits our data acquisition range. In order to gain a better insight into the nature of this emission, we have measured the emission lifetimes at different wavelengths. As shown in the inset of Fig. 3b for five representative wavelengths, contrary to the case of Ge-oxide related visible emission, the near-infrared decay traces are described by single exponential decay functions with microsecond decay times in a range of 18–24 μs. We believe that the observation of long-lived, intense emission in ultra-pure Ge nanoparticles strongly suggests that the nature of light emission relies on indirect optical transitions in the core of oxygen-passivated Ge particles. According to this picture, the measured increase in the emission lifetime with increasing wavelength could be explained by the stronger non-radiative multi-phonon coupling (higher phonon density of states) for the shorter emission wavelengths, which are more separated in energy from the indirect Ge band-gap. However, the interplay between radiative and non-radiative recombination in this novel nanoscale Ge system will be specifically investigated in subsequent contributions.

## 4. Conclusion

In this work we have successfully synthesized ultra-pure germanium nanoparticles (30 nm average crystallite size and negligible micro-strain of 0.058%) and we have investigated their photoluminescence behavior under visible laser excitation. This material demonstrates two distinctive emission bands, consisting of a weak, short-lived (0.5–1 ns), emission around 500 nm (associated with GeO) and an intense, long-lived (~20 μs), near-infrared emission at 1575 nm due to pure Ge. We believe that the controlled fabrication of ultra-pure Ge nanoparticles could lead to a demonstration of novel light emitting devices which leverage the strong light scattering properties of nanoscale pure Ge powders.

## Acknowledgements

The authors thank Drs. Scott Speakman, Elizabeth Shaw, and Anthony Garrett-Reed of the Center for Material Science and Engineering at MIT for in-depth analysis of the powder XRD, XPS and TEM results, respectively. This project was partially funded by the AFOSR under MURI Award No. FA9550-06-1-0470. This work also made use of the MRSEC Shared Experimental Facilities at

MIT, supported by the National Science Foundation under Award Number DMR-02-13282.

## References

[1] A. Puzder, A.J. Williamson, J.C. Grossman, G. Galli, J. Chem. Phys. 117 (2002) 6721.
[2] E.W. Draeger, J.C. Grossman, A.J. Williamson, G. Galli, Phys. Rev. Lett. 90 (2003) 167402-1.
[3] L. Pavesi, D.J. Lockwood (Eds.), Silicon Photonics, Springer-Verlag, Berlin, 2004.
[4] L. Pavesi, S. Gaponenko, L. Dal Negro (Eds.), Towards the First Silicon Laser, NATO Science Series, Kluwer Academic, Dordrecht, 2003.
[5] A. Puzder, A.J. Williamson, F.A. Reboredo, G. Galli, Phys. Rev. Lett. 91 (2003) 157405-1.
[6] M.V. Wolkin, J. Jorne, P.M. Fauchet, G. Allan, C. Delerue, Phys. Rev. Lett. 82 (1999) 197.
[7] L. Pavesi, L. Dal Negro, C. Mazzoleni, G. Franzò, F. Priolo, Nature 408 (2000) 440.
[8] Y.M. Niquet, G. Allan, C. Delerue, M. Lannoo, Appl. Phys. Lett. 77 (2000) 1182.
[9] S. Yerci, M. Kulakci, U. Serincan, M. Shandalov, Y. Golan, R. Turan, J. Nanosci. Nanotechnol. 8 (2008) 759.
[10] M. Larsson, A. Elfving, P.O. Holtz, G.V. Hansson, W.X. Ni, Surf. Sci. 532 (2003) 832.
[11] S. Takeoka, M. Fujii, S. Hayashi, K. Yamamoto, Appl. Phys. Lett. 74 (1999) 1558.
[12] G. Taraschi, S. Saini, W.W. Fan, L.C. Kimerling, E.A. Fitzgerald, J. Appl. Phys. 93 (2003) 9988.
[13] G. Kartopu, V.A. Karavanskii, U. Serincan, R. Turan, R.E. Hummel, Y. Ekinci, A. Gunnaes, T.G. Finstad, Phys. Status Solidi A 202 (2005) 1472.
[14] W. Wang, K. Wang, D. Han, B. Poudel, X. Wang, D.Z. Wang, B. Zeng, Z.F. Ren, Nanotechnology 18 (2007) 075707.
[15] A. Killian, T.F. Morse, Aerosol Sci. Technol. 34 (2001) 227–235.
[16] J.I. Langford, A.J.C. Wilson, J. Appl. Crystallogr. 11 (1978) 102–113.
[17] H.P. Klug, L.E. Alexander, X-ray Diffraction Procedures for Polycrystalline and Amorphous Materials, Wiley and Sons, 1974.
[18] B. Briggs, M.P. Seah, Practical Surface Analysis by Auger and X-ray Photoelectron Spectroscopy, John Wiley & Sons Ltd., Berlin, 1983.
[19] R.W.G. Wyckoff, Crystal Structures, second ed., Interscience, 1963.
[20] G. Kartopu, S.C. Bayliss, V.A. Karavanskii, R.J. Curry, R. Turan, A.V. Sapelkin, J. Lumin. 101 (2003) 275–283.